CHEMISTRY OF MATERIALS

ARTICLE

pubs.acs.org/cm

Rare Earth Hexaboride Nanowires: General Synthetic Design and Analysis Using Atom Probe Tomography

Joseph R. Brewer,[†] Robert M. Jacobberger,[†] David R. Diercks,[‡] and Chin Li Cheung*[,†,§]

[†]Department of Chemistry and [§]Nebraska Center for Materials and Nanosciences, University of Nebraska, Lincoln, Nebraska 68588, United States

[‡]University of North Texas, Denton, Texas 76207, United States

Supporting Information

ABSTRACT: A general synthetic design for a wide range of single-crystalline rare earth hexaboride nanowires (REB_6, RE = Y, La, Ce, Pr, Nd, Sm, Gd, Tb, Dy, Ho) was established using palladium-nanoparticle-assisted chemical vapor deposition and examined by atom probe tomography analysis. Insights from binary phase diagrams were demonstrated to determine proper catalyst choice and vapor−liquid−solid growth conditions for this wide range of binary wire systems. High-resolution transmission electron microscopy indicated that these nanowires were single-crystalline with diameters of about 50 nm and lengths of several micrometers. Atom probe tomography analysis revealed that these nanowires were of high purity and correct stoichiometry. No detectable palladium diffusion was found beyond the first several nanometers of the catalyst nanoparticle−nanowire interface.

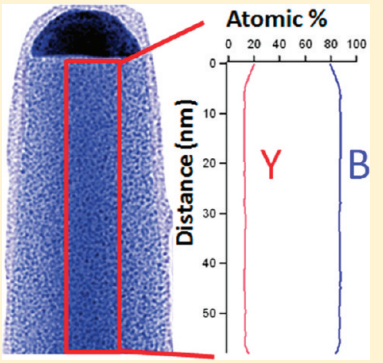

KEYWORDS: rare earth hexaboride, nanowire, atom probe tomography

1. INTRODUCTION

Rare-earth hexaborides (REB_6) have received renewed research interest in recent years because these materials have high melting points[1] and a variety of unique physical properties including superconductivity,[2−4] semiconductivity,[5] fluctuating valence,[6−8] metal−insulator transition,[8,9] and low work function.[10−13] Because of the rigidity of the octahedral boron cage, lattice matching is nearly perfect across the entire range of REB_6 materials, leading to the possibility of tuning their electronic properties through RE dopants.[13,14] Hence, REB_6 nanomaterials can potentially motivate new designs of high-temperature nanoelectronic devices with enhanced electron collection and injection properties.[15]

Reported synthetic methods for metal hexaboride nanowires via either a vapor−liquid−solid (VLS) mechanism[16−21] or a vapor-solid (VS) mechanism[22,23] differ considerably in the choice of catalysts and precursors for boron and metal chemical sources. These methods, though shown to work effectively in individual cases, have not been proven effective over the entire range of REB_6 because of limited chemical analysis of as-synthesized materials and after-reaction catalyst particles. Thus, there is limited understanding of the catalysts' roles in the growth process. Knowledge of potential impurities and unbalanced stoichiometry in these VLS- and VS-grown REB_6 nanowires can improve our understanding of the electronic properties and implementation of these nanowire elements into nanoscale electronic devices. Nonetheless, such information is currently not available in the literature due to the limitations of conventional analytical techniques to accurately quantify their compositions. For example, the use of typical energy dispersive X-ray spectroscopy (EDS) of boron content is complicated by the fluorescence and preferential absorption of light element X-rays by the samples, especially ones containing high-z elements.[24]

Atom probe tomography (APT) is an analytical technique that allows mapping of the composition of materials at the atomic scale typically with sub-100 ppm sensitivity through sequential evaporation events from individual atomic planes.[25−28] APT has recently been applied to identify the profiles of intentional dopants[29] and unintentional dopants from the catalyst particles[30] in VLS-grown nanowires. These studies have provided valuable understanding of the relationship between the dopant profiles and their electron transport behavior, but so far have been applied only to a few selected Group IV and III−V nanowire systems. This article reports our effort toward the development of a general VLS synthesis for REB_6 nanowires (RE = Y, La, Ce, Pr, Nd, Sm, Gd, Tb, Dy, Ho) by chemical vapor deposition (CVD) and the use of consecutive transmission electron microscopy (TEM) and APT analysis of nanowires[31] for synthetic feedback.

2. EXPERIMENTAL SECTION

2.1. Vapor−Liquid−Solid Growth of REB_6 Nanowires. REB_6 (RE = Y, La, Ce, Pr, Nd, Sm, Gd, Tb, Dy, Ho) nanowires were synthesized by a CVD scheme via the VLS mechanism using metal chlorides, decaborane, and palladium (Pd) nanoparticles, similar to our previous method.[18] Briefly, Pd nanoparticles were drop-coated onto

Received: January 26, 2011
Revised: April 7, 2011
Published: April 20, 2011

(100) silicon (Si) wafer substrates, placed on a quartz reactor boat along with a rare earth trichloride ($RECl_3$) powder, and then loaded into a 1"-diameter quartz tube in a horizontal tube furnace. The reaction was carried out at 1000 °C and 100 mTorr under a 20 standard cubic centimeter per minute (SCCM) of argon and 0.75 SCCM of decaborane flow mixture. The $RECl_3$ was located in the colder, upstream section of the reactor at a temperature between 700 and 850 °C. Experiments for LaB_6 nanowire synthesis were also performed on single-side polished (100) magnesium oxide (MgO) single crystals (MTI Co., Richmond, CA). Similar results were obtained as in the case with Si substrates.

2.2. Characterization of REB_6 Nanowires. The morphology of the as-synthesized REB_6 nanowire films and cross-sections were studied by field-emission scanning electron microscopy (FE-SEM) on a Hitachi S4700 operated at 15 keV (Hitachi High Technologies America, Inc., Pleasanton, CA). The crystal structures of these nanowires were characterized by bright field TEM on a Tecnai G^2 F20 S-Twin operated at 200 keV (FEI, Hillsboro, OR) and by selected area electron diffraction (SAED). The elemental compositions of three different regions of the nanowires (catalyst particles at the nanowire tips, bulk and side edge of the wires) were analyzed by EDS. X-ray diffractometry (XRD) (Rigaku D/Max-B Diffractometer, Rigaku Americas, The Woodlands, TX) was also conducted to examine the crystallinity and crystal structure of the bulk nanowire samples on the Si substrates. The weighted average wavelength of the Cu Kα X-ray source is 1.5417 Å.

Atom probe tomography (APT) using a LEAP 3000X HR (CAMECA Atom Probe Technology Center, Madison, WI) was applied to determine the atomic compositions and structures of four different types of nanowires (YB_6, LaB_6, HoB_6, and SmB_6) using a consecutive TEM-APT analysis technique.[31] Individual nanowire samples were mounted on TEM grids using a dual beam (focus ion beam (FIB)/SEM) system (FEI Nova 200 NanoLab, FEI, Hillsboro, OR) Autoprobe 250 nanomanipulator (Omniprobe, Inc., Dallas, TX) as described previously.[2] TEM images of the nanowire materials before and after APT analysis were captured to provide accurate geometric parameters for the reconstructions of nanowires using the IVAS software. The atom probe analyses were carried out on a LEAP 3000X HR using laser pulsed mode with a 532 nm wavelength laser, 0.1−1.4 nJ laser energy and 100−200 kHz pulse repetition rate at temperatures of 16 to 40 K.

3. RESULTS AND DISCUSSION

The RE-B binary phase diagrams and the binary phase diagrams of the catalyst with each elemental component of the REB_6 systems[32] were examined to determine an appropriate catalyst for VLS growth of all REB_6 nanowire systems considered. These REB_6 binary phase diagrams can be divided into two regions outside of the hexaboride phase: (1) metal-rich/boron-deficient region in which several different stable crystalline phases coexist and (2) metal-deficient/boron-rich region in which usually only hexaboride and boron coexist, along with dodecaboride for some RE elements. It is logical to conjecture that catalysts with high boron solubility would be advantageous in minimizing the formation of metal-rich VLS-grown REB_6 nanowires.

Synthetic methods utilizing the VLS growth model for REB_6 nanowire synthesis typically focus on Au and Pt catalyst particles, probably because they were the first two catalysts to demonstrate LaB_6 whisker growth.[16] It was noted in this study that B has much lower solubility in Au than in Pt. However, no information regarding the interaction between Pt and RE was available at that time. Furthermore, few reports in recent literature have attempted to expound these findings or make attempts to understand why these catalysts are effective or what traits might yield

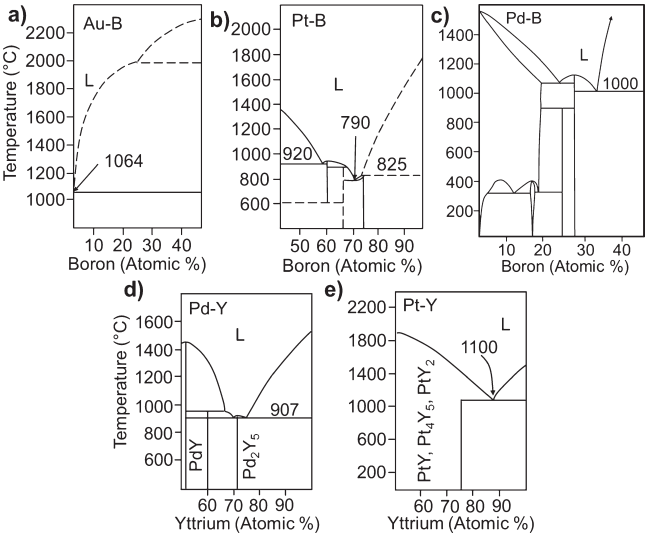

Figure 1. Abridged binary phase diagrams depicting lowest melting point eutectics of (a) Au−B, (b) Pt−B, (c) Pd−B, (d) Pd−Y, and (e) Pt−Y.[32].

improved VLS catalysts. For example, from the binary phase diagrams for the Au−B, Pt−B, and Pd−B binary system (Figure 1a−c), Pd and Pt can dissolve a much higher percentage of B than Au. Comparisons among them also indicate that the Pt−B system has a much lower liquid eutectic temperature than that of the Pd−B system. However, the solubility of the RE element in the catalyst also plays a significant role in the growth of these REB_6 systems. As an illustration of this, consider the synthesis of YB_6 nanowires. In this case, according to the Pd−Y and Pt−Y binary phase diagrams (Figure 1d,e), Y has only sufficient solubility in Pd, not Pt, below 1100 °C. This suggests that Pd might serve as a general synthesis catalyst material for VLS growth of REB_6 nanowires at lower temperatures than Pt. Upon comparisons among all RE-Pd phase diagrams,[32] a reaction temperature of 1000 °C was chosen for the growth conditions due to the solubility limits of B in Pd (Figure 1c).

To confirm our analysis of the binary phase diagrams for predicting VLS growth conditions of REB_6 nanowire systems, we conducted the synthesis of YB_6 utilizing Pt and Pd nanoparticles on Si wafer substrates in separate CVD experiments at 1000 and 1090 °C under similar experimental conditions described previously.[18] At 1000 °C, the Pt catalyzed substrate yields only a thin film while there is significant growth of YB_6 nanowires on the Pd catalyzed substrate (Figure 2a and 2b). This is likely due to the lack of yttrium solubility in Pt at 1000 °C. However, at an increased reaction temperature of 1090 °C, closer to the liquid eutectic temperature of Pt−Y, YB_6 nanowires can be synthesized using Pt nanoparticles (Figure 2c). This temperature study provides circumstantial evidence that the solubility of the individual components in the catalyst particles plays a vital role in determining VLS-growth conditions for REB_6 nanowires.

Our VLS-growth methodology with Pd nanoparticles was also successfully applied to the synthesis of most known REB_6 systems (RE = Y, La, Ce, Pr, Nd, Sm, Gd, Tb, Dy, Ho) (Figure 3). Morphology, single-crystalline nature and [100] growth orientations of these nanowires were confirmed by high resolution TEM (HRTEM) and SAED data on dozens of nanowires from each demonstrated REB_6 system. Figure 4 depicts typical TEM images of YB_6 and LaB_6 nanowires

dx.doi.org/10.1021/cm200258h |Chem. Mater. 2011, 23, 2606–2610

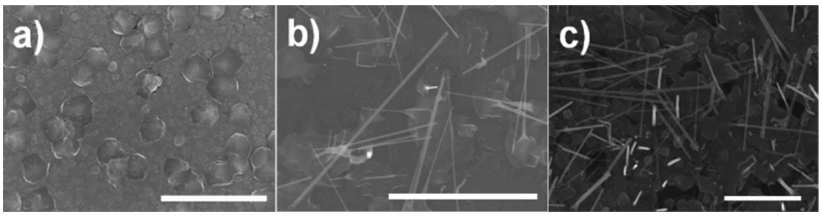

Figure 2. Scanning electron microscopy (SEM) images of YB_6 nanostructures synthesized at 1000 °C with (a) Pt nanoparticles and (b) Pd nanoparticles, and (c) at 1090 °C with Pt nanoparticles. Scale bars are 5 μm.

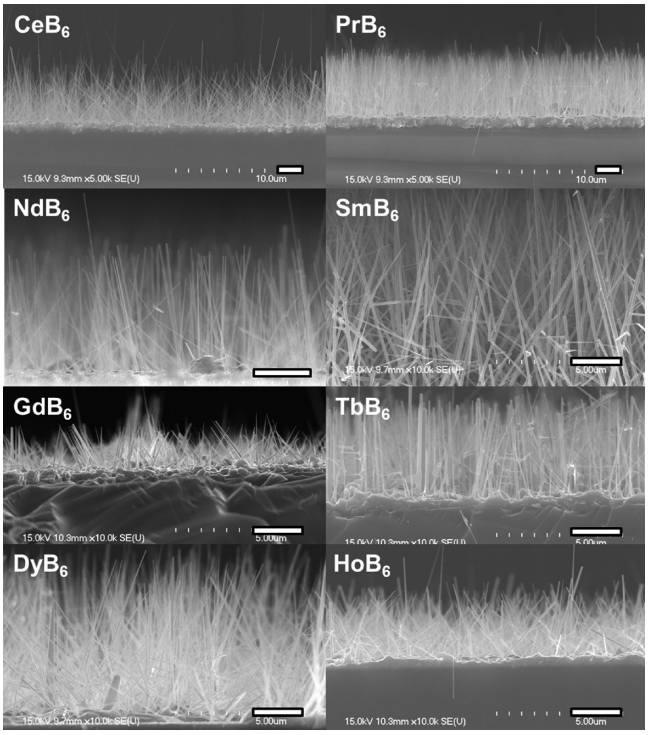

Figure 3. SEM images of Pd-catalyzed CVD-grown rare earth boride nanowire samples on Si wafer substrates. All scale bars are 2 μm.

synthesized through the Pd-catalyzed reactions. These REB_6 nanowires typically have diameters less than 50 nm and lengths of several micrometers. HRTEM images of these nanowires also depict dark particles located at the tips of these wires and a thin amorphous layer, typically less than 2 nm, on their sidewalls. XRD patterns for nine of the REB_6 (RE = Y, La, Ce, Pr, Nd, Sm, Gd, Tb, Dy) nanowire films reveal only the corresponding REB_6 diffraction patterns. Though the XRD pattern of the HoB_6 nanowire film shows a mixture of REB_4 and REB_6 patterns, both HRTEM images and SAED patterns of the examined nanowires from this sample indicate the presence of HoB_6 nanowires. (See the Supporting Information for detailed structure and composition characterization data of the 10 described REB_6 systems.)

Because of the low atomic number of boron and the high atomic number of the RE elements, determination of nanowire stoichiometry by ZAF corrected EDS appears to be highly inaccurate. Therefore, APT was employed to determine REB_6 compositions. Figure 5 represents the APT 3D reconstruction analysis of a LaB_6 nanowire and a catalyst particle at the tip of a LaB_6 nanowire after the reaction. Individual nanowires were mounted on the posts of sectioned TEM grids in a SEM using a

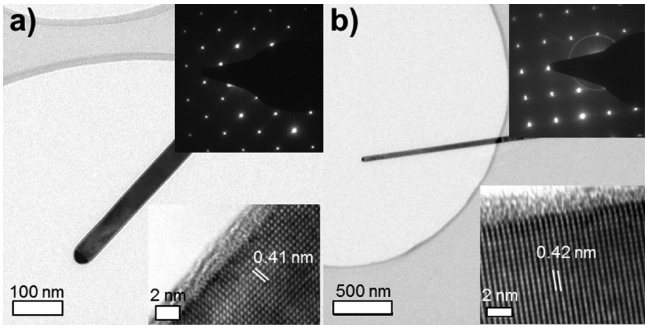

Figure 4. TEM images of (a) YB_6 nanowire and (b) LaB_6 nanowire. Insets are (top) SAED patterns and (bottom) HRTEM images of the corresponding nanowires.

nanomanipulator.[31] This allows access to HRTEM imaging of the samples and verification of the morphology and structures of the REB_6 materials before and after the APT analysis, providing complementary information and assisting in creating accurate APT reconstructions. The mass spectra data of the LaB_6 nanowire from the APT analysis suggest that only La and B are detected in the bulk of the nanowire with the Pd signal below the detection limit of 100 ppm. This implies that an insignificant (below the detection limit) amount of Pd may have diffused from the catalyst particle tip to the nanowire. We do acknowledge that the chemical compositions of the Pd catalyst nanoparticles during the reaction may be different from those after the reaction. However, analysis of the post-run catalyst particles may shed some details on the possible nanowire growth process. From the APT analysis, the postreaction catalyst particle at the nanowire tip is composed mostly of Pd and Si mainly in the form of $PdSi_x$, but also has some regions of nearly pure Si. This indicates that Si from the substrate can also be dissolved into the Pd catalyst at the reaction temperature. The $PdSi_x$ and Si regions then likely form upon cooling after the nanowire growth. The content of both La and B are less than 5 at % in the catalyst particle, confirming the expected VLS-growth mechanism. No detectable Si is found in this nanowire. To evaluate the significance of Si substrates in the catalytic growth, LaB_6 nanowires were synthesized similarly on (100) MgO single crystal substrates which do not alloy with Pd. Similar nanowire growth results were obtained with MgO substrates (see Figure S15 in the Supporting Information). This suggests that Si substrates are not required in the formation of the REB_6 nanowires.

The diffusion of Pd atoms from the catalyst particle into a LaB_6 nanowire can be examined qualitatively in panels d and g in Figure 5. The presence of Pd atoms is not detectable beyond 2 nm from the interface of the wire and particle, suggesting that Pd is an excellent catalyst choice for synthesizing high-purity REB_6

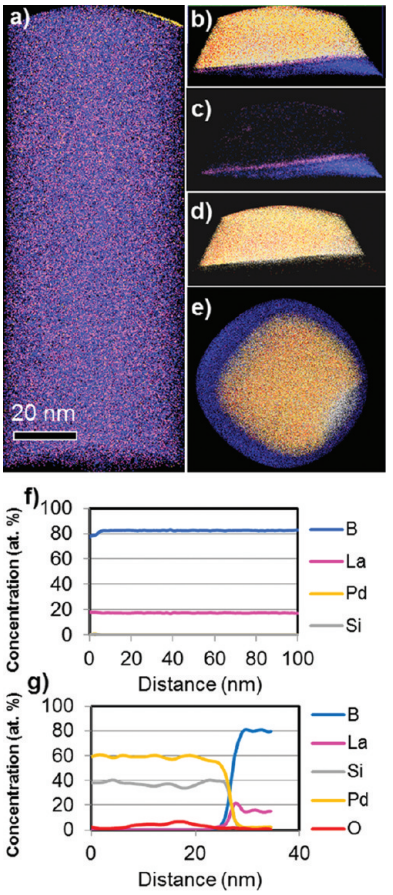

Figure 5. APT reconstruction of a VLS-grown LaB_6 nanowire and a catalyst particle at the nanowire tip after the VLS growth: (a) nanowire and (b−e) catalyst particle. Figure 5b is a complete reconstruction of the particle. Two additional representations of the particle are shown to indicate the locations of (c) La and B and (d) Pd, Si and O. Figure 5e is a top view. Color scheme: La (purple), B (blue), Si (gray), O (red), and Pd (yellow). (f) 1D *z*-axis concentration profile of the wire in a. (g) 1D *z*-axis concentration profile for the catalyst particle in b. "0 nm" refers to the top of the particle. The nanowire-catalyst interface is located at ~26 nm from the top.

Table 1. Summary of Boron Composition Results from APT and EDS Analysis for Four REB_6 Nanowire Systems

REB_6	at % B, APT	at % B, EDS (uncorrected)	at % B, EDS (ZAF corrected)
YB_6	84.9	98.7	8.8
LaB_6	86.2	98.8	44.1
SmB_6	79.7	98.0	4.2
HoB_6	84.6	97.4	1.2

nanowires. Also of interest is the apparent high concentration of La at the interface of the catalyst and nanowire. The likely cause is a precipitation event upon cooling of the system below the liquid eutectic temperature. This feature can also be identified in the HRTEM images of nanowire-catalyst interfaces (see the Supporting Information).

Measured atomic composition results confirm that the ratios of RE:B are indeed 1:6, which provide a better compositional match to the crystallographic determinations by TEM than by EDS or ZAF corrected EDS (Table 1). Similar to the LaB_6 nanowires, the axial and lateral concentration profiles of a YB_6 nanowire also indicate a high metal composition at the interface and an almost uniform stoichiometry along the length of the wire and from the center of the nanowire to the edge (see Figure S16 in the Supporting Information). Though a slight increase in B content can be identified at the edges of the wire in the concentration profiles, it is unlikely that the increase is large enough to indicate a different phase. Thus, amorphous layers identified under TEM are likely surface adsorbates rather than amorphous B generated during the CVD process.

Of the four REB_6 systems in which APT analysis was applied, only the SmB_6 nanowire has a stoichiometry different from that predicted from the RE-B binary phase diagram. This can be attributed to the significant "tailing" of the boron peaks in the APT mass spectra, indicating that B evaporation occurred even after the peak energy of the laser pulse (see Figure S17 in the Supporting Information). There was also an increase in the number of multiple simultaneous hits on the ion detector during the APT analysis of SmB_6 versus those of the other three REB_6 systems. Both observations suggest that B may have been undercounted if B was possibly evaporating between laser pulses or several B ions reached the detector simultaneously. One possible cause may be due to differences in charge transport in these nanowire systems. SmB_6 has holes as the major charge carriers, whereas the other three analyzed systems (YB_6, LaB_6, HoB_6) all have electrons as the major charge carriers.[33,34] During the generation of the positive ions in the laser evaporation process, electrons need to be drawn from the evaporated surface. Materials with holes as the major charge carriers may be inefficient at electron transport, leading to possible resistive heating and evaporation events continuing for a prolonged period between the laser pulses.

4. CONCLUSION

In conclusion, we have demonstrated a general synthetic route for a wide range of single-crystalline REB_6 nanowires using Pd nanoparticles. These successful results illustrate insights from previous findings[35] that binary phase diagrams can be used to determine proper catalyst choice and VLS-growth conditions for binary wire systems. APT analysis is shown to provide access to the determination of accurate boron content in these REB_6 nanowire systems and feedback to advance the understanding of the role of the Pd catalyst nanoparticles in the demonstrated growth process. With the availability of accurate quantitative compositional information and a versatile catalyst for nearly all REB_6 systems, the use of low work function REB_6 nanowires and the exploration of nanoscale magnetic and electrical transport phenomena with doped REB_6 systems in nanoscale electronic applications may begin to be fully realized.

■ ASSOCIATED CONTENT

Supporting Information. Experimental details and characterization data. This material is available free of charge via the Internet at http://pubs.acs.org

■ AUTHOR INFORMATION

Corresponding Author
*E-mail: ccheung2@unl.edu.

■ ACKNOWLEDGMENT

The financial support is from the Maude Hammond Fling Faculty Research Fellowship at UNL. R.M.J. thanks NASA Nebraska EPSCoR for his fellowship support. We thank the Center of Biotechnology at UNL and the Center for Advanced Research and Technology at UNT for the use of their facilities.

■ REFERENCES

(1) Balakrishnan, G.; Lees, M. R.; Paul, D. McK. *J. Magn. Magn. Mater.* **2004**, *272−276*, 601–602.
(2) Hiebl, K.; Sienko, M. J. *Inorg. Chem.* **1980**, *19*, 2179–2180.
(3) Fisk, Z.; Schmidt, P. H.; Longinotti, L. D. *Mater. Res. Bull.* **1976**, *11*, 1019–1022.
(4) Schell, G.; Winter, H.; Rietschel, H.; Gompf, F. *Phys. Rev. B* **1982**, *25*, 1589–1599.
(5) Mercurio, J. P.; Etourneau, J.; Naslain, R.; Hagenmuller, P. *J. Less-Common Met.* **1976**, *47*, 175–180.
(6) Kebede, A.; Aronson, M. C.; Buford, C. M.; Canfield, P. C.; Cho, J. H.; Coles, B. R.; Cooley, J. C.; Coulter, J. Y.; Fisk, Z.; Goettee, J. D.; Hults, W. L.; Lacerda, A.; McLendon, T. D.; Tiwari, P.; Smith, J. L. *Phys. B.: Condens. Matter* **1996**, *223−224*, 256–259.
(7) Wachter, P. In *Handbook on the Physics and Chemistry of Rare Earths*; K.A.Gschneider, J.; Eyring, L., Eds.; North-Holland: Amsterdam, 1994; Vol. 19, p 177.
(8) Derr, J.; Knebel, G.; Braithwaite, D.; Salce, B.; Flouquet, J.; Flachbart, K.; Gabáni, S.; Shitsevalova, N. *Phys. Rev. B* **2008**, *77*, 193107.
(9) Farkašovský, P. *Phys. Rev. B* **1995**, *51*, 1507.
(10) Gesley, M.; Swanson, L. W. *Surf. Sci.* **1984**, *146*, 583–599.
(11) Swanson, L. W.; Gesley, M. A.; Davis, P. R. *Surf. Sci.* **1981**, *107*, 263–289.
(12) Uijttewaal, M. A.; de Wijs, G. A.; de Groot, R. A. *J. Phys. Chem. B* **2006**, *110*, 18459–18465.
(13) Schmidt, P. H.; Joy, D. C. *J. Vac. Sci. Technol.* **1978**, *15*, 1809–1810.
(14) Tarascon, J. M.; Isikawa, Y.; Chevalier, B.; Etoumeau, J.; Hagenmuller, P.; Kasaya, M. *J. Phys. France* **1980**, *41*, 1135–1140.
(15) Zhang, H.; Tang, J.; Yuan, J.; Ma, J.; Shinya, N.; Nakajima, K.; Murakami, H.; Ohkubo, T.; Qin, L. C. *Nano Lett.* **2010**, *10*, 3539–3544.
(16) Givargizov, E. I.; Obolenskaya, L. N. *J. Less-Common Met.* **1986**, *117*, 97–103.
(17) Brewer, J. R.; Deo, N.; Wang, Y. M.; Cheung, C. L. *Chem. Mater.* **2007**, *19*, 6379–6381.
(18) Wang, G. H.; Brewer, J. R.; Chan, J. Y.; Diercks, D. R.; Cheung, C. L. *J. Phys. Chem. C* **2009**, *113*, 10446–10451.
(19) Jash, P.; Nicholls, A. W.; Ruoff, R. S.; Trenary, M. *Nano Lett.* **2008**, *8*, 3794–3798.
(20) Zhang, H.; Zhang, Q.; Zhao, G. P.; Tang, J.; Zhou, O.; Qin, L. C. *J. Am. Chem. Soc.* **2005**, *127*, 13120–13121.
(21) Amin, S. S.; Li, S.-y.; Roth, J. R.; Xu, T. T. *Chem. Mater.* **2009**, *21*, 763–770.
(22) Xu, J.; Zhao, Y.; Zou, C.; Ding, Q. *J. Solid State Chem.* **2007**, *180*, 2577–2580.
(23) Xu, J. Q.; Zhao, Y. M.; Shi, Z. D.; Zou, C. Y.; Ding, Q. W. *J. Cryst. Growth* **2008**, *310*, 3443–3447.
(24) McGee, J. J.; Slack, J. F.; Herrington, C. R. *Am. Mineral.* **1991**, *76*, 681–684.
(25) Seidman, D. N. *Annu. Rev. Mater. Res.* **2007**, *37*, 127–158.
(26) Kelly, T. F.; Larson, D. J.; Thompson, K.; Alvis, R. L.; Bunton, J. H.; Olson, J. D.; Gorman, B. P. *Annu. Rev. Mater. Res.* **2007**, *37*, 681–727.
(27) Kelly, T. F.; Miller, M. K. *Rev. Sci. Instrum.* **2007**, *78*, 031101.
(28) Seidman, D. N.; Stiller, K. *MRS Bull.* **2009**, *34*, 717–724.
(29) Perea, D. E.; Hemesath, E. R.; Schwalbach, E. J.; Lensch-Falk, J. L.; Voorhees, P. W.; Lauhon, L. J. *Nat. Nanotechnol.* **2009**, *4*, 315–319.
(30) Perea, D. E.; Allen, J. E.; May, S. J.; Wessels, B. W.; Seidman, D. N.; Lauhon, L. J. *Nano Lett.* **2006**, *6*, 181–185.
(31) Diercks, D.; Gorman, B.P.; Cheung, C. L.; Wang, G. *Microsc. Microanal.* **2009**, *15* (Suppl. 2), 254–255.
(32) Massalski, T. B.; Okamoto, H.; Subramanian, P. R.; Kacprzak, L. *Binary Alloy Phase Diagrams*, 2nd ed.; ASM International: Materials Park, OH, 1990.
(33) Nickerson, J. C.; White, R. M.; Lee, K. N.; Bachmann, R.; Gegalle, T. H.; Hull, G. W., Jr. *Phys. Rev. B* **1971**, *3*, 2030–2042.
(34) Paderno, Y. B.; Novikov, V. I.; Garf, E. S. *Powder Metall. Met. Ceram.* **1969**, *8*, 921–923.
(35) Duan, X. F.; Lieber, C. M. *Adv. Mater.* **2000**, *12*, 298–302.